Materials Research. 2017; 20(2): 487-495
DOI: http://dx.doi.org/10.1590/1980-5373-MR-2016-0214

N and F Codoped TiO_2 Thin Films on Stainless Steel for Photoelectrocatalytic Removal of Cyanide Ions in Aqueous Solutions

Edgar Leonardo Castellanos-Leal[a], Próspero Acevedo-Peña[b]*, Viviana Raquel Güiza-Argüello[c], Elcy María Córdoba-Tuta[a,c]

[a] *Grupo de Investigaciones en Minerales, Biohidrometalurgia y Ambiente, Universidad Industrial de Santander, Bucaramanga, Colombia*
[b] *CONACyT-Centro de Investigación en Ciencia Aplicada y Tecnología Avanzada, Unidad Legaria, IPN, 11500. Mexico City, Mexico*
[c] *Grupo de Investigación en Desarrollo y Tecnología de Nuevos Materiales, Universidad Industrial de Santander, Bucaramanga, Colombia*

Received: March 10, 2016; Revised: December 30, 2016; Accepted: January 25, 2017

N-F codoped TiO_2 films were immobilized on stainless steel sheets through a combined approach involving a dip-coating technique and a hydrothermal treatment, followed by calcination at 400°C in the presence of air. Photocatalyst characterization was conducted using XRD, Raman and UV-VIS spectroscopy as well as SEM. The films were tested in a three-electrode cell for the photoelectrocatalytic degradation of CN-containing compounds. The results showed that the increase in the degradation rate of CN-containing compounds is both influenced by a synergistic effect of the doping agents and strongly dependent on the concentration of CN-containing compounds in the solution. Nitrogen contributed to the enhanced photoactivity under visible light due to the generation of localized states within the band gap of TiO_2, whereas the presence of fluoride improved the superficial properties of the film, which resulted in higher amounts of CN-containing compounds that were degraded by direct charge transfer through the photogenerated holes.

Keywords: *Codoped TiO_2, non-metallic doping, photoelectrocatalysis, cyanide oxidation*

1. Introduction

Currently, contamination of natural water sources due to industrial toxic waste is one of the major environmental and social global issues[1]. In this sense, the gold mining industry is one of the largest water polluter in the world, due to its heavy use of toxic substances such as cyanide, which are disposed of into natural water sources. Conventional methods for the removal of cyanide involve chemical oxidation with various substances, which include hydrogen peroxide, chloride dioxide, ozonation, and SO_2/air, among others. However, the limitations associated with these methods, such as high cost of reagents and/or equipment as well as the generation of new products with high toxicity[2], has motivated the study of photoelectrocatalysis as an alternative technique for the detoxification of cyanide waters.

In this context, photoelectrocatalysis (PEC) using semiconductor materials such as titanium oxide (TiO_2), which is low-cost, chemically stable and quantum efficient[3], has emerged as one of the most promising advanced oxidation processes for the removal of contaminants from natural water sources. In order to perform TiO_2 PEC, photon illumination with a wavelength equal or less than 388 nm is required, which corresponds to the ultraviolet (UV) region and promotes the generation of electron-hole pairs that contribute to the redox process[3-5]. However, the sunlight spectrum has its maximum radiation between 400-700 nm, and only a small fraction of this range corresponds to UV light. This hinders the ability to use solar radiation in PEC processes on TiO_2 films. Therefore, in order to address this problem and avoid the use of artificial UV lamps, it is essential to develop strategies towards the reduction of the band-gap of the semiconductor[6-8].

In this context, doping with non-metallic elements such as N, F, C, S and B[9-20] has become an attractive alternative because this type of modification results in materials with a low recombination rate, great chemical stability and good response to visible light, relative to metallic doping[3, 21]. Recently, it has been suggested that the use of codoped systems such as N and F[13,15,19,20], N and B[14], and N and V[16] allow to compensate for the excess charge from substitutional doping with N. Additionally, these codoped materials are effectively used in the charge separation of photogenerated electrons and holes, improving photoelectrocatalytic activity[13-16,19,20]. In this regard, the combination of N and F appears as an interesting doping approach, since it would not only increase the TiO_2 response due to the presence of N[13,15,19,20], but also would improve the superficial and crystallinity properties of the material due to modification with F[13,15,19,20]. Nonetheless,

* e-mail: prosperoster@gmail.com

the mechanisms of action of N and F as doping agents in TiO_2 are strongly dependent on the methods for the synthesis and preparation of the photocatalysts.

Furthermore, even though the use of this type of semiconductor materials for the photoelectrocatalytic oxidation of cyanide represents a promising technology for the decontamination of natural water sources, it has hardly been investigated[5,22]. To our knowledge, the studies reported in the literature primarily deal with the electrooxidation of CN^- by direct electron transfer[23,24] using expensive electrodes, which compromises the economical feasibility of the process. In the present work, we attempt to gain deeper insights into the CN^- photoelectrocatalytic oxidation processes that involve the use of TiO_2 semiconductor films[5,22] supported on low-cost substrates. Simultaneous doping of TiO_2 with N and F was performed and its effect on photoactivity under visible light was evaluated. Moreover, the influence of e^--h^+ pairs and oxidative species such as OH* radicals on process efficiency was also assessed. The photoelectrochemical studies presented here lay important groundwork needed to accurately understand the mechanisms involved in the photoelectrolytic oxidation of cyanide towards the development of low-cost and efficient technologies for the removal of CN^- from contaminated natural water sources.

2. Experimental

2.1. Preparation of N-F codoped TiO_2 films

Semiconductor films were prepared as previously described[12]. Briefly, 5 mL of titanium tetraisopropoxide (TTIP) were dissolved in 5 mL of isopropanol, followed by combination with a second solution consisting of 5 mL of acetyl acetone (AcAc) and 0.6 mL of HNO_3 (65%) in 30 mL of distilled water. The resulting mixture was stirred for 12 h at room temperature. After this, 5 mL of triethylamine (TEA) and 0.93 g of NH_4F were added as nitrogen and fluorine sources, respectively. Stirring was kept for an additional 12 h. AISI 304 stainless steel substrates were prepared by abrasion with SiC #600 paper followed by cleaning in an ultrasonic bath with ethanol and then acetone, 15 min each time. The films were formed on the metallic substrates by dip-coating and then placed into an autoclave for 4 h at 17 psi and 125 °C. Finally, the photocatalyst films were annealed at 400 °C for 1 h. Following similar procedures as the one described above, four types of films were prepared: i) without doping agents (pristine TiO_2), ii) with TEA (TiO_2-T), iii) with NH_4F (TiO_2-NF), and iv) codoped TiO_2 (TiO_2-TNF). Although the stainless steel is prone to corrosion, it can be used to manufacture photoanodes as long as the semiconductor film deposited on such a substrate is homogeneous, stable chemically and has corrosion protective properties, such as occurs with sol-gel TiO_2 coatings[25-27].

2.2. Characterization of the supported photocatalysts

Grazing angle X-ray diffraction (GAXRD) with an incidence angle of 3° was performed on a BRUKER D8 diffractometer. Additionally, the films were characterized by Raman spectroscopy using a HORIBA Scientific HR LabRAM Evolution equipped with a green laser (532 nm) and a 50X objective. Attenuated reflectance infrared spectroscopy (ATR-FTIR) analyses were performed on a NICOLET IS50 (Thermo Scientific) at a resolution of 4 cm^{-1} with 32 scans and an interferometer speed of 0.4147 $cm\,s^{-1}$. Moreover, the morphology of the supported photocatalysts was examined by field-emission scanning electron microscopy (FE-SEM) using a FEI QUANTA FEG 650 microscope, and film roughness was evaluated with an AFM Park NX10 microscope using contact mode in 20 μm × 20 μm areas.

2.3. Photoelectrocatalytic oxidation of cyanide solutions

The experiments were performed using a conventional three-electrode cell. AISI 304 stainless steel sheets (4 cm^2) coated with the semiconductor films served as the working electrode. A saturated calomel electrode [SCE: Hg/Hg_2Cl_2 (saturated KCl)] in a Luggin capillary was used as the reference electrode, and the counter electrode consisted of a high purity graphite rod (AGKSP grade, Alfa Aesar). All measurements were carried out on a GAMRY 600 potentiostat. Illumination was provided by a 150 W metal-halide lamp (Phillips MHN-TD UV block) with an integrated UV light filter. 25 mL of solution [NaCN (50, 100 and 250 ppm CN^-) + 0.1 M Na_2SO_4] of pH 11 were used. Solution pH was kept constant by addition of NaOH. The levels of cyanide were measured by duplicate using titration with silver nitrate in a Tritroline Easy automatic titrator (SI analytics). All solutions were prepared using deionized water, and all reagents were analytic grade (Merck).

3. Results and discussion

3.1. Characterization of the photocatalyst films

In the context of photoelectrochemistry, and especially for macroelectrolysis purposes, it is essential to ensure that the working electrode is stable and exhibits appropriate structural properties. This is particularly crucial when working with semiconductor films supported on substrates of different nature, as it is the case in the present studies (TiO_2/stainless steel). Therefore, SEM characterization was performed in order to evaluate the morphology of the synthesized films (Figure 1). The representative SEM images in Figure 1 evidence the superficial line patterns associated with SiC paper abrasion during preparation of the metal

substrates. Despite this, all four types of films appeared to have a crack-free, homogeneous and compact structure, features that are required for their use as photoanodes since they favor their stability and increase corrosion resistance of the metal substrate[25,26,28,29].

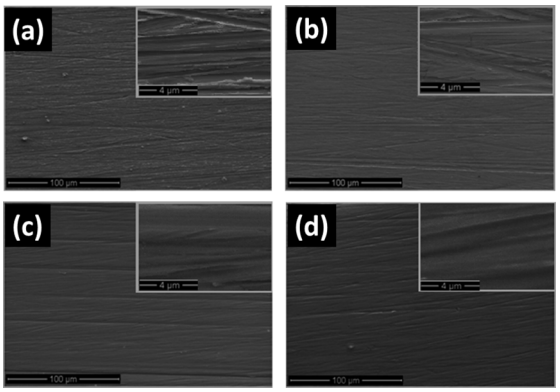

Figure 1. SEM images for (a) pristine TiO_2, (b) TiO_2-T, (c) TiO_2-NF and (d) TiO_2-TNF films.

Additionally, AFM images obtained for the films in contact mode (20 µm × 20 µm area) are shown in Figure 2. As it can be noted, polishing patterns caused by abrasion with SiC paper (# 600) are present on all the films. However, some agglomerates are observed as a function of the composition of the films. Average (R_a) and root mean squared (R_q) roughnesses are tabulated in Table 1. The addition of TEA seems to promote the increase of roughness (TiO_2-T and TiO_2-TNF); while NH_4F appears to favor the formation of more homogeneous and thicker films, which increases their corrosion protective character[27].

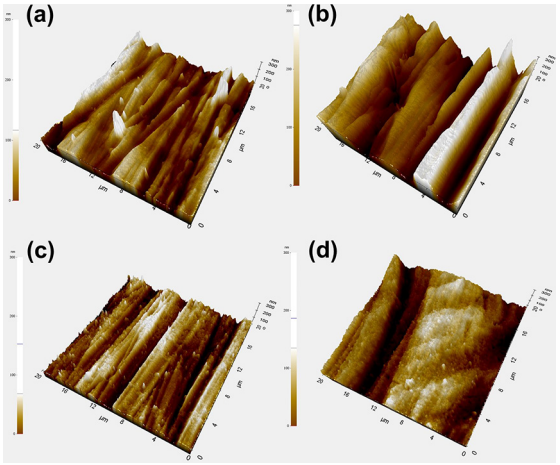

Figure 2. AFM images for the synthesized films on stainless steel: a) pristine TiO_2; b) TiO_2 T; c) TiO_2 NF and d) TiO_2 TNF.

Grazing angle X-ray diffraction (GAXRD) patterns for the different films are shown in Figure 3. All four samples were subjected to hydrothermal treatment for 4 h followed by calcination at 400°C. As it can be observed in Figure 3,

Table 1. Roughness measurements for TiO_2 and modified TiO_2 films supported on stainless steel.

Material	Roughness	
	R_a (nm)	R_q (nm)
Pristine TiO_2	44.1	59.4
TiO_2-T	112.7	140.5
TiO_2-NF	28.2	34.7
TiO_2-TNF	57.2	68.9

anatase is the only TiO_2 crystalline phase that is present, which is known as the phase with the highest activity in photocatalytic processes[3]. Moreover, the intense peak associated with Fe content in stainless steel was detected, due to the thin nature of the TiO_2 films. Some additional diffraction peaks associated with iron nitride ($FeN_{0.0324}$) were also observed for the TiO_2-NF sample.

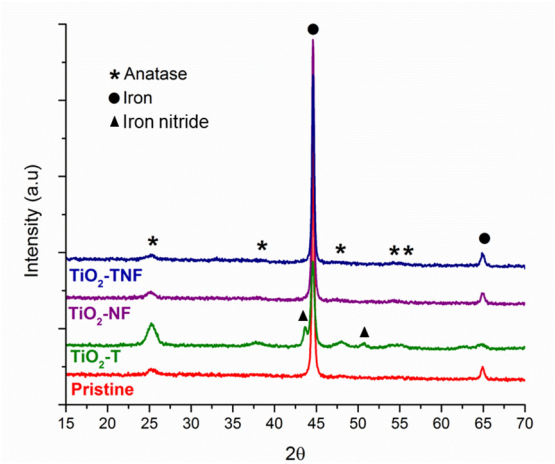

Figure 3. X-ray diffraction patterns for pristine TiO_2, TiO_2-T, TiO_2-NF and TiO_2-TNF films after hydrothermal treatment and annealing at 400 °C.

The optical response of semiconductor materials can be related to the presence of energetic states within their band-gap, which are induced by defects and/or the effect of doping elements on the structure of TiO_2. Such localized states are generated above the lower limit of the valence band (type *p* doping) or below the upper limit of the conduction band (type *n* doping) and are responsible for the absorption of less energetic light. This allows the activation of TiO_2 under visible light[9-20]. Figure 4 shows the UV-VIS spectra for the films, which reveal that modifications with the doping agents significantly affected the visible light absorption of the TiO_2-NF and TiO_2-TNF samples. Using the Kubelka-Munk modified function (see Figure 4 insert) the band-gap values for each photocatalyst were estimated[30] as follows: 3.2 eV for pristine TiO_2, 3.1 eV for TiO_2-T and 2.9 eV for both TiO_2-NF and TiO_2-TNF. These results indicate that when TEA is used alone, the insertion of N in the oxide network is not stable to heat treatment, which leaves anionic vacancies

in the material. On the other hand, modification with either NH_4F or TEA and NH_4F resulted in more thermally stable doping of TiO_2, and therefore, produced a material that can effectively use visible light in photo-assisted electrochemical processes for the degradation of contaminants.

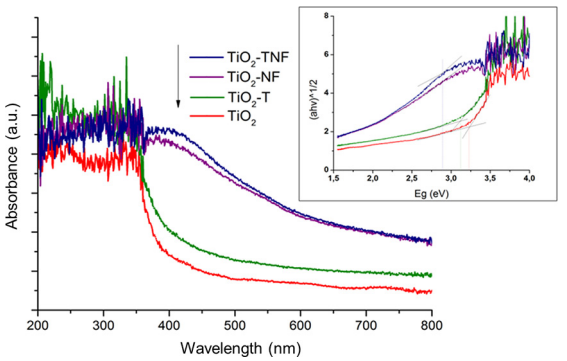

Figure 4. UV-VIS spectra for TiO_2 pristine, TiO_2-T, TiO_2-NF and TiO_2-TNF films after hydrothermal treatment and annealing at 400 °C.

Figure 5 shows the ATR-FTIR spectra for the synthesized films. TiO_2 characteristic bands can be identified for all samples. The band at 3350 cm^{-1} can be attributed to the stretching of the OH groups from residual alcohol, hydroxyl groups (Ti-OH)[31-33] as well as from water that was trapped in the oxide network. The band between 1800-1500 cm^{-1} represents the contribution due to water proton absorption[31-33], and the band between 871-479 cm^{-1} corresponds to Ti-O-Ti bonding[31-33].

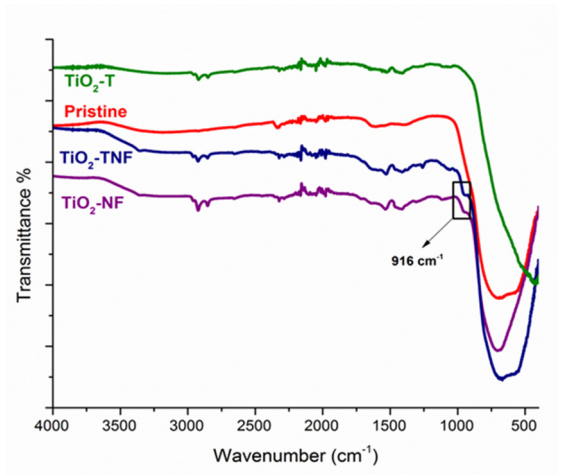

Figure 5. ATR-FTIR spectra for TiO_2 pristine, TiO_2-T, TiO_2-NF and TiO_2-TNF films after hydrothermal treatment and annealing at 400 °C.

Additionally, for the modified samples (TiO_2-T, TiO_2-NF and TiO_2-TNF) a signal at 1458 cm^{-1} was detected. This band is associated with $–NO_x$ groups (-Ti-O-N-Ti-), which indicates incorporation of N in the TiO_2 structure. As expected, such signal was very weak for the TiO_2-T film due to the lack of thermal stability of the N inserted in this sample. This is consistent with what has been previously reported in the literature, which indicates that the N contribution from TEA can leave from the oxide structure at calcination temperatures around 400 °C[34]. Furthermore, a small band at 916 cm^{-1} was only detected for the samples that contained fluoride (TiO_2-NF and TiO_2-TNF) which is attributed to TiO_6 octahedral distortion resulting from N and F incorporation in the TiO_2 oxide network[31-33].

The results from Raman characterization are shown in Figure 6. As it can be observed, all the film samples exhibited the characteristic bands for the vibrational modes of the anatase phase: E_g (148 cm^{-1}), B_{1g} (396 cm^{-1}), A_{1g} (513 cm^{-1}) and E_g (638 cm^{-1})[35]. Relative to pristine TiO_2, a slight shift in the main band of the E_g mode (148 cm^{-1}) was observed for the doped samples. This could be due to the presence of structural defects in the TiO_2 network. The red shift observed for TiO_2-T (E_g = 146 cm^{-1}, see Figure 6 insert) can be associated with a variation in the crystal size[35,36]. On the other hand, the blue shift detected for TiO_2-NF (E_g =152 cm^{-1}) and TiO_2-TNF (E_g =153 cm^{-1}) has been previously attributed to distortions in the TiO_2 crystal network caused by the presence of N and F, which increase the vibration energy of the E_g mode[35,36].

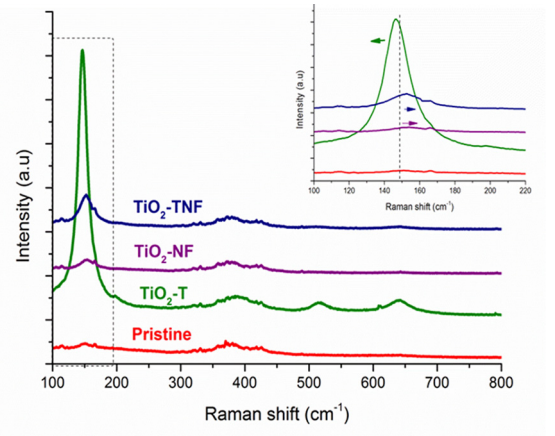

Figure 6. Raman spectra for TiO_2 pristine, TiO_2-T, TiO_2-NF and TiO_2-TNF films after hydrothermal treatment and annealing at 400 °C.

3.2. Semiconducting properties

In order to evaluate the impact of the modifying agents on the semiconducting properties of the synthesized thin films, Mott-Schottky (M-S) plots were generated at a frequency of 400 Hz (Figure 7)[37]. A positive slope in the linear region of the M-S plots can be observed for all cases, which indicates the *n-type* behavior of the films. The linear region in Figure 7 was fitted to equation (1) (solid line) in order to estimate the flat-band potential (E_{fb}) and donor density (N_d) of the formed films, which are summarized in Table 2:

$$\frac{1}{C_{sc}^2} = \frac{2N_A}{N_d F \varepsilon_r \varepsilon_0} \cdot \left(E_m - E_{fb} - \frac{RT}{F} \right) \quad (1)$$

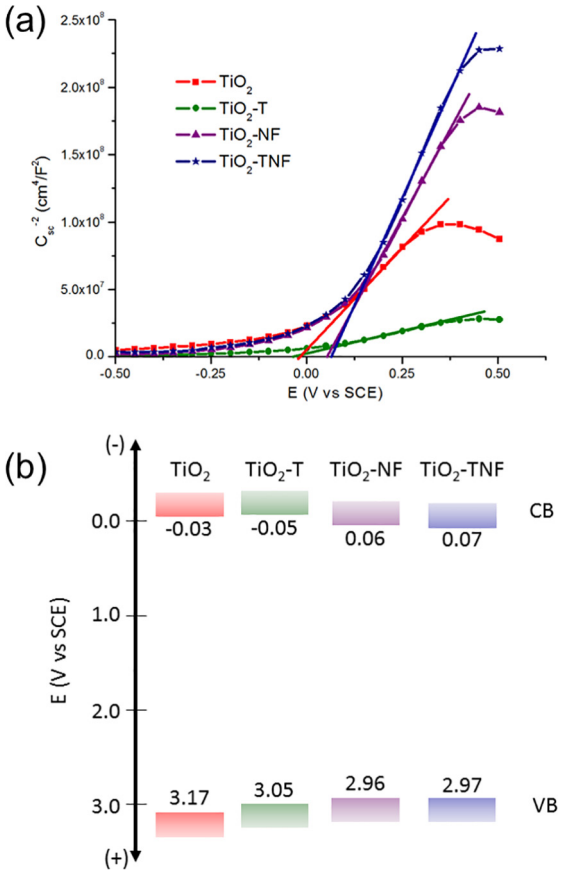

Figure 7. (a) Mott-Schottky plots for the synthesized films obtained experimentally at a frequency of 400 Hz in a 0.1 M Na_2SO_4 (pH 11), and (b) Band diagram derived by assuming the flat band potential of the films as the potential of the conduction band (CB). Valence band (VB) position was estimated by adding the measured band gap energy (Figure 4).

Table 2. Donor density (N_d) and flat band potential (E_{fb}) estimated from Figure 7.

Sample	$N_d \times 10^{21}$ cm^{-3}	E_{fb} mV Vs SCE
TiO_2	2.4	-33
TiO_2-T	11.7	-49
TiO_2-NF	1.4	61
TiO_2-TNF	1.1	71

where N_A is Avogadro's number (6.02×10^{23} mol^{-1}), N_d (cm^{-3}) is the donor density, F is the Faraday constant ($\sim 9.65 \times 10^4$ C mol^{-1}), ε_r is the relative permittivity (50)[37], ε_0 is the permittivity of vacuum (8.8542×10^{-14} F cm^{-1}), E_m (V) is the potential at which the measurement was carried out, E_{fb} (V) is the flat-band potential, R is the gas constant (8.314 JK^{-1} mol^{-1}), and T is the absolute temperature ($\sim$ 298 K). The third term in parentheses can be assumed to be negligible at room temperature, relative to the other terms.

As seen in Table 2, relative to pristine TiO_2, TEA modification of TiO_2 (TiO_2-T) resulted in a slight shift towards more negative values of E_{fb} with a nearly five-fold increase in the donor density (N_d), which indicated the generation of defects such as oxygen vacancies in the material[9,10]. On the other hand, NH_4F doping (TiO_2-NF) displaced the flat band potential towards positive values, with a slight decrease in N_d, compared to what was measured for the pristine samples. This behavior could be related to the compensating effect associated with the presence of F, which prevents the generation of new defects such as oxygen vacancies when N and F are simultaneously incorporated in the TiO_2 structure[13]. Moreover, it is well known that fluorine chemisorption onto a TiO_2 surface changes the surface acidity of the material, which could explain the variation in the E_{fb} values relative to pristine TiO_2. Furthermore, band diagrams were sketched from E_{fb} measurements, see Figure 7b. The valence band position (VB), derived by adding the band-gap energy (measured from UV-vis spectra in Figure 4), shows a slight displacement toward lower potential values for N-modified films. This behavior indicates that N2p states are being generated by the incorporation of N in the TiO_2 lattice, as it has been previously proposed[5].

3.3. Photoelectrocatalytic oxidation of cyanide

Synthesized films were used as photoanodes in a conventional three-electrode cell to perform the photoelectrocatalytic oxidation of cyanide in synthetic solutions. All experiments were carried out in solutions of pH 11. Solution pH was kept constant by addition of 0.1 M NaOH to avoid the generation of hydrogen cyanide. In order to determine the most favorable potentiostatic conditions for the photoelectrocatalytic oxidation of cyanide, TEA and NH_4F modified TiO_2 films (TiO_2-TNF) were used to degrade 100 ppm of CN^- at different potentials for 120 min (see Figure 8). As shown in Figure 8, the percentage of degraded CN^- increases proportionally with the imposed potential, exceeding 50% cyanide oxidation when a potential of 0.97 V Vs SCE is reached. However, beyond this point, cyanide degradation drops drastically to undetectable levels at 1.1 V Vs SCE. When looking at the currents that were registered during the experiment, a different trend is observed: there is a monotonic increase of the current followed by a change in the slope of the curve in the interval of potentials where maximum percentage CN^- degradation is achieved (0.95 to 0.97 V). This response indicates that potentials above 0.97 V favor an additional process that reduces the efficiency of CN^- degradation, which is possibly the oxidation of water. Based on these findings, a potential of 0.97 V Vs SCE was selected for the photoelectrocatalytic oxidation of the cyanide solutions.

Once the appropriate potential was selected, four different film samples were prepared (pristine TiO_2, TiO_2-T, TiO_2-NF and TiO_2-TNF) for the PEC oxidation of 100 ppm of CN^- during 150 min, as shown in Figure 9.

The kinetic curves in Figure 9a reveal that the highest degradation rate was achieved on the TiO_2 films modified with TEA and NH_4F (TiO_2-TNF), which allowed for up to

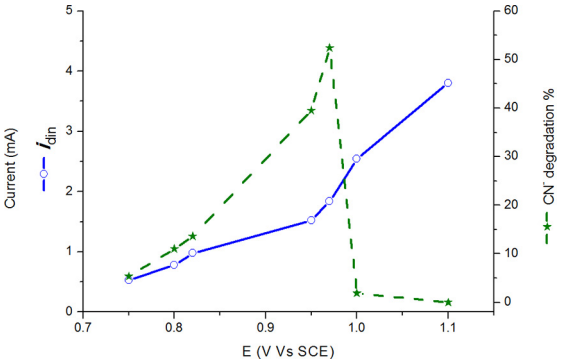

Figure 8. Photoelectrocatalytic oxidation of CN^- (100 ppm, pH=11) on TiO_2 TNF film during 120 minutes.

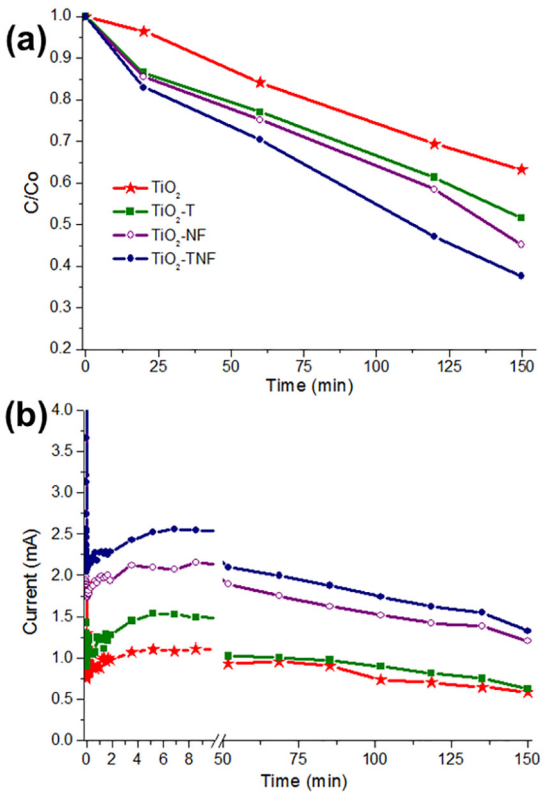

Figure 9. Photoelectrocatalytic oxidation of CN^- (100 ppm, pH=11) on pristine TiO_2, TiO_2-T, TiO_2-NF and TiO_2-TNF films during 150 minutes: a) kinetic curves and b) current transients.

64% CN^- degradation after 2 hr. The remaining TiO_2-NF, TiO_2-T and pristine TiO_2 samples provided a 55 %, 48 % and 32 % CN^- removal, respectively. Furthermore, Figure 9b shows the cronoamperograms generated during the PEC experiments. In all cases, there is a drastic current drop followed by an increase until a maximum current value is reached, and then it slowly falls down to the end of the test. In previous studies, it was observed that the variation of the current with time is related to the morphology of the films, i.e. their thickness and porosity[5]. Nonetheless, for the present studies, the magnitude of the current varied significantly among samples despite the fact that all films exhibited similar morphology. As shown in Figure 9b, the oxidation process occurs at a higher rate on the TiO_2-TNF and TiO_2-NF films, relative to pristine TiO_2 and TiO_2-T. These results are consistent with what was observed for the kinetic curves and confirm that simultaneous modification of TiO_2 with TEA and NH_4F results in a codoped material with a higher ability for photoelectrocatalytic oxidation of CN^-, relative to pristine or individually modified TiO_2.

As seen in Figure 10a, increasing CN^- concentrations increased the quantity of degraded cyanide in both photoelectrocatalytic (PEC) and electrocatalytic (EC) processes. Figure 10 shows that the amount of oxidized cyanide was directly related to the magnitude of the registered currents, according to Faraday's law of electrolysis. Moreover, regardless of the contaminant initial concentration, illumination resulted in higher CN^- removal and therefore higher currents were generated, relative to the process without illumination (Figure 10b). This is associated with the generation of electron-hole pairs on the surface of the semiconductor[5,38]. As it has been previously reported in the literature[5,22-24], photocatalytic oxidation of CN^- on TiO_2 occurs primarily due to direct charge transfer.

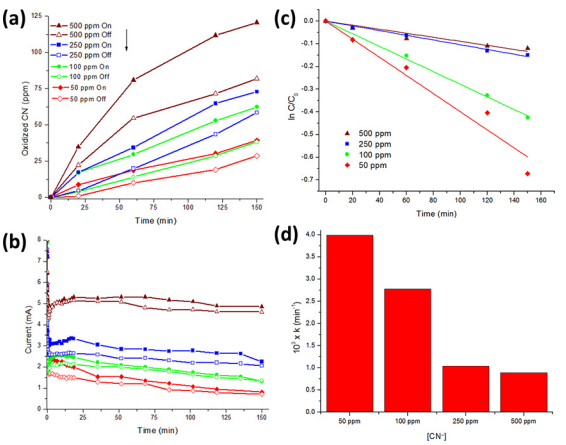

Figure 10. (a) Photoelectrocatalytic (On) and electrocatalytic (Off) oxidation of CN^- at different concentrations vs. time, and (b) current transients. (c) $\ln(C/C_0)$ vs. Time for photoelectrocatalytic process at different cyanide concentrations. (d) Effect of the cyanide concentration over the kinetic constant (k) for pseudo-first order reaction[5].

Furthermore, $\ln C/C_0$ vs time curves obtained at different initial cyanide concentrations, and the kinetic constant for a pseudo-first order reaction versus the initial cyanide concentration are plotted in figures 10c and 10d, respectively. The higher k values were obtained at the lowest cyanide concentration, which indicates that photoelectrocatalytic process could be employed more efficiently at a low pollutant concentration, as it has been stated for photocatalytic processes[3].

Since TiO_2 modification with fluoride generally results in an increased generation of OH^* radicals for both photocatalytic

(PC) and photoelectrocatalytic (PEC) processes, the effect of OH^* radicals on PEC cyanide degradation was evaluated. In order to do this, 80 mM of tertbutanol (t-BuOH) was added to the CN^- solution[38]. A constant potential of 0.97 V Vs SCE under illumination for 150 min was used as well. Figure 11 shows the results for the TiO_2-TNF and TiO_2-T films. The kinetic curves indicate a small decrease in CN^- degradation when OH^* radicals are inhibited by t-BuOH, due to the fact that oxidation occurs primarily by direct electron transfer.

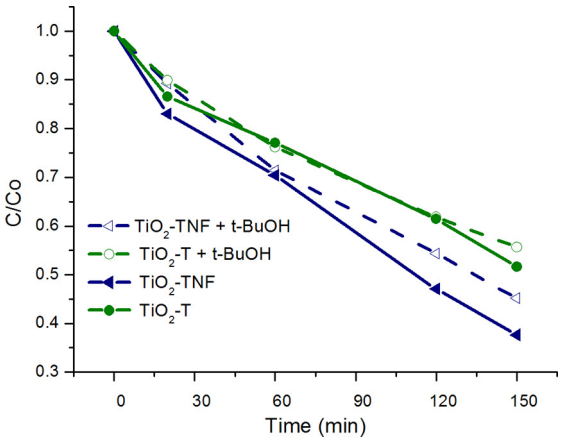

Figure 11. Effect of t-BuOH scavenger on the rate of CN^- degradation on TiO_2-TNF and TiO_2-T films.

Several researchers have associated the photocatalytic oxidation of CN^- on TiO_2 with a direct charge transfer process[39-43]. Nonetheless, it has also been reported that such photocatalytic oxidation could also take place through indirect mechanisms at the semiconductor/electrolyte interface. These indirect mechanisms are due to the presence of adsorbed hydroxyl ions that form OH^* radicals or caused by a homogeneous phase reaction with the OH^* radicals that diffuse into the cyanide solution[3]. These OH^* radicals react with the CN^- ions to give cyanate ions (OCN^-) and formamide ($HCONH_2$)[39]. However, most authors report that for the carbon balance after degradation, the sum of CN^- and OCN^- ion concentrations is constant and properly fits the mass balance[39,40]. For this reason, indirect oxidation mechanisms do not seem feasible, or do not take place at significant magnitudes during the photocatalytic oxidation of CN^-.

4. Conclusions

TiO_2 modification using nitrogen and fluoride precursors (TEA and NH_4F) revealed a higher degree of crystallinity of the anatase phase and superior absorption of visible light, relative to pristine TiO_2. This modification probably favored a direct oxidation mechanism through the holes trapped on the catalyst (≡Ti-O*), which resulted in a more efficient use of visible light to generate electron-hole pairs.

The results from the PEC experiments showed that TEA and NH_4F modified TiO_2 photoanodes (TiO_2-TNF) achieve a significant degradation percentage of cyanide (> 60%) in diluted solutions (100 ppm) in just 150 min, when an optimal potential of 0.97 V Vs. SCE is used. Furthermore, it was found that the generation of OH* radicals during TiO_2 modification with fluoride does not have a significant effect on the PEC degradation of CN^- ions, which takes place by direct electron transfer. Cumulatively, these results indicate that the increase in percentage degradation of cyanide can be associated with a more efficient use of visible light due to a reduction in the band-gap of TiO_2 in the presence of NH_4F and TEA.

5. Acknowledgements

The authors would like to acknowledge financial support from COLCIENCIAS (Project 1102-521-28875) and Universidad Industrial de Santander (DIEF Ingenierías Fisicoquímicas, Project 9416). The authors would also like to thank Dr. Hugo A. Estupiñán from Universidad Nacional de Colombia (Medellín) for technical assistance with AFM measurements.

6. References

1. Mert BK, Sivrioğlu Ö, Yonar T, Özçiftçi S. Treatment of Jewelry Manufacturing Effluent Containing Cyanide Using Oxone-Based Photochemical Advanced Oxidation Processes. *Ozone: Science & Engineering*. 2014;36(2):196-205.

2. Parga JR, Vázquez V, Valenzuela JL, Matamoros Z, González G. Detoxification of cyanide using titanium dioxide and hydrocyclone sparger with chlorine dioxide. *Chemical Speciation & Bioavailability*. 2012;24(3):176-182.

3. Henderson MA. A surface science perspective on TiO_2 photocatalysis. *Surface Science Reports*. 2011;66(6-7):185-297.

4. Peralta-Ruiz YY, Lizcano-Beltrán EM, Laverde D, Acevedo-Peña P, Córdoba EM. Formation of TiO_2 photoanodes by simultaneous electrophoretic deposition of anatase and rutile particles for photoassisted electrolytic copper ions removal. *Química Nova*. 2012;35(3):499-504.

5. Ramírez-Santos AA, Acevedo-Peña P, Córdoba EM. Photo-assisted electrochemical copper removal from cyanide solutions using porous TiO_2 thin film photo-anodes. *Materials Research*. 2014;17(1):69-77.

6. Kumar SG, Devi LV. Review on Modified TiO_2 Photocatalysis under UV/Visible Light: Selected Results and Related Mechanisms on Interfacial Charge Carrier Transfer Dynamics. *The Journal of Physical Chemistry A*. 2011;115(46):13211-13241.

7. Pelaez M, Nolan NT, Pillai SC, Seery MK, Falaras P, Kontos AG, et al. A review on the visible light active titanium dioxide photocatalysts for environmental applications. *Applied Catalysis B: Enviromental*. 2012;125:331-349.

8. Fagan R, McCormack DE, Dionysiou DD, Pillai SC. A review of solar and visible light active TiO_2 photocatalysis for treating bacteria, cyanotoxins and contaminants of emerging concern. *Materials Science in Semiconductor Processing*. 2016;42(Pt 1):2-14.

9. Asahi R, Morikawa T, Ohwaki T, Aoki K, Taga Y. Visible-Light Photocatalysis in Nitrogen-Doped Titanium Oxides. *Science*. 2001;293(5528):269-271.

10. Sathish M, Viswanathan B, Viswanath RP, Gopinath S. Synthesis, Characterization, Electronic Structure, and Photocatalytic Activity of Nitrogen-Doped TiO_2 Nanocatalyst. *Chemistry of Materials*. 2005;17(25):6349-6353.

11. Yu J, Wang W, Cheng B, Su BL. Enhancement of Photocatalytic Activity of Mesporous TiO_2 Powders by Hydrothermal Surface Fluorination Treatment. *The Journal of Physical Chemistry C*. 2009;113(16):6743-6750.

12. Wu D, Long M, Cai W, Chen C, Wu Y. Low temperature hydrothermal synthesis of N-doped TiO_2 photocatalyst with high visible-light activity. *Journal of Alloys and Compounds*. 2010;502(2):289-294.

13. Giannakas AE, Seristatidou E, Deligiannakis Y, Konstantinou I. Photocatalytic activity of N-doped and N-F co-doped TiO_2 and reduction of chromium(VI) in aqueous solution: An EPR study. *Applied Catalysis B: Environmental*. 2013;132-133:460-468.

14. Uddin N, Shibly SUA, Ovali R, Islam S, Mazumder MR, Islam S, et al. An experimental and first-principles study of the effect of B/N doping in TiO_2 thin films for visible light photo-catalysis. *Journal of Photochemistry and Photobiology A: Chemistry*. 2013;254:25-34.

15. Hamilton JWJ, Byrne JA, Dunlop PSM, Dionysiou DD, Pelaez M, O'Shea K, et al. Evaluating the Mechanism of Visible Light Activity for N,F-TiO_2 Using Photoelectrochemistry. *Journal of the Physical Chemistry C*. 2014;118(23):12206-12215.

16. Zhong J, Xu J, Wang Q. Nitrogen and vanadium Co-doped TiO_2 mesosponge layers for enhancement in visible photocatalytic activity. *Applied Surface Science*. 2014;315:131-137.

17. Samsudin EM, Abd Hamid SB, Juan JC, Basirun WJ, Centi G. Enhanced of the intrinsic photocatalytic activity of TiO_2 in the degradation of 1,3,5-triazine herbicides by doping with N,F. *Chemical Engineering Journal*. 2015;280:330-343.

18. Li H, Hao Y, Lu H, Liang L, Wang Y, Qiu J, et al. A systematic study on visible-light N-doped TiO_2 photocatalyst obtained from ethylenediamine by sol-gel method. *Applied Surface Science*. 2015;344:112-118.

19. Zhang Y, Han C, Nadagouda MN, Dionysiou DD. The fabrication of innovative single crystal N,F-codoped titanium dioxide nanowires with enhanced photocatalytic activity for degradation of atrazine. *Applied Catalysis B: Environmental*. 2015;168-169:550-558.

20. He X, Aker WG, Pelaez M, Lin Y, Dionysiou DD, Hwang H. Assessment of nitrogen-fluorine-codoped TiO_2 under visible light for degradation of BPA: Implication for field remediation. *Journal of Photochemistry and Photobiology A: Chemistry*. 2016;314:81-92.

21. Ma X, Wu Y, Lu Y, Xu J, Wang Y, Zhu Y. Effect of Compensated Codoping on the Photoelectrochemical Properties of Anatase TiO_2 Photocatalyst. *The Journal of Physical Chemistry C*. 2011;115(34):16963-16969.

22. Zhao X, Zhang J, Qu J. Photoelectrocatalytic oxidation of Cu-cyanides and Cu-EDTA at TiO_2 nanotube electrode. *Electrochimica Acta*. 2015;180:129-137.

23. Lanza MRV, Bertazzoli R. Selection of a Commercial Anode Oxide Coating for Electro-oxidation of Cyanide. *Journal of the Brazilian Chemical Society*. 2002;13(3):345-351.

24. Felix-Navarro RM, Lin SW, Violante-Delgadillo V, Zizumbo-López A, Pérez-Sicarios S. Cyanide Degradation by Direct and Indirect Electrochemical Oxidation in Electro-active Support Electrolyte Aqueous Solutions. *Journal of the Mexican Chemical Society*. 2011;55(1):51-56.

25. Wang D, Bierwagen GP. Sol–gel coatings on metals for corrosion protection. *Progress in Organic Coatings*. 2009;64(4):327-338.

26. Ćurković L, Ćurković HO, Salopek S, Renjo MM, Šegota S. Enhancement of corrosion protection of AISI 304 stainless steel by nanostructured sol–gel TiO_2 films. *Corrosion Science*. 2013;77:176-184.

27. Léonard GLM, Remy S, Heinrichs B. Overview of Superhydrophilic, Photocatalytic and Anticorrosive Properties of TiO_2 Thin Films Doped with Multi-walled Carbon Nanotubes and Deposited on 316L Stainless Steel. *Materials Today: Proceedings*. 2016;3(2):434-438.

28. Shinde PS, Go GH, Lee J. Multilayered large-area WO_3 films on sheet and mesh-type stainless steel substrates for photoelectrochemical hydrogen generation. *International Journal of Energy Research*. 2013;37(4):323-330.

29. Nikkanen JP, Huttunen-Saarivita E, Salminen T, Hyvärinen L, Honkanen M, Isotahdon E, et al. Enhanced photoactive and photoelectrochemical properties of TiO_2 sol-gel coated steel by the application of SiO_2 intermediate layer. *Applied Catalysis B: Environmental*. 2015;174-175:533-543.

30. Gärtner M, Ballmann J, Damm C, Heinemann FW, Kisch H. Support-controlled chemoselective olefin–imine addition photocatalyzed by cadmium sulfide on a zinc sulfide carrier. *Photochemistry and Photobiology Sciences*. 2007;6(2):159-164.

31. Yu J, Su Y, Cheng B, Zhou M. Effects of pH on the microstructures and photocatalytic activity of mesoporous nanocrystalline titania powders prepared via hydrothermal method. *Journal of Molecular Catalysis A: Chemical*. 2006;258(1-2):104-112.

32. Bu XZ, Zhang GK, Gao YY, Yang YQ. Preparation and photocatalytic properties of visible light responsive N-doped TiO_2/rectorite composites. *Microporous and Mesoporous Materials*. 2010;136(1-3):132-137.

33. Jiang Y, Luo Y, Zhang F, Guo L, Ni L. Equilibrium and kinetic studies of C.I. Basic Blue 41 adsorption onto N, F-codoped flower-like TiO_2 microspheres. *Applied Surface Science*. 2013;273:448-456.

34. Téllez LA, Díaz FA. *Síntesis de TiO_2 dopado con nitrógeno con actividad fotocatalítica bajo luz visible*. [Bachelor thesis]. Bucaramanga: Universidad Industrial de Santander; 2010.

35. Xu CY, Zhang PX, Yan L. Blue shift of Raman peak from coated TiO_2 nanoparticles. *Journal of Raman Spectroscopy*. 2001;32(10):862-865.

36. Wang J, Zhang P, Li X, Zhu J, Li H. Synchronical pollutant degradation and H_2 production on a Ti^{3+}-doped TiO_2 visible photocatalyst with dominant (001) facets. *Applied Catalysis B: Environmental*. 2013;134-135:198-204.

37. Acevedo-Peña P, Carrera-Crespo JE, González F, González I. Effect of heat treatment on the crystal phase composition, semiconducting properties and photoelectrocatalytic color removal efficiency of TiO_2 nanotube arrays. *Electrochimica Acta*. 2014;140:564-571.

38. Yin L, Niu J, Shen Z, Chen J. Mechanism of Reductive Decomposition of Pentachlorophenol by Ti-Doped β-Bi_2O_3 under Visible Light Irradiation. *Environmental Science and Technology*. 2010;44(14):5581-5586.

39. Augugliaro V, Blanco-Gálvez J, Cáceres-Vásquez J, García-López E, Loddo V, López-Muñoz MJ, et al. Photocatalytic oxidation of cyanide in aqueous TiO_2 suspensions irradiated by sunlight in mild and strong oxidant conditions. *Catalysis Today*. 1999;54(2-3):245-253.

40. Chiang K, Amal R, Tran T. Photocatalytic oxidation of cyanide: kinetic and mechanistic studies. *Journal of Molecular Catalysis A: Chemical*. 2003;193(1-2):285-297.

41. Osathaphan K, Chucherdwatanasak B, Rachdawong P, Sharma VK. Photocatalytic oxidation of cyanide in aqueous titanium dioxide suspensions: Effect of ethylenediaminetetracetate. *Solar Energy*. 2008;82(11):1031-1036.

42. Pala A, Politi RR, Kurşun G, Erol M, Bakal F, Öner G, et al. Photocatalytic degradation of cyanide in wastewater using new generated nano-thin film photocatalyst. *Surface and Coating Technology*. 2015;271:207-216.

43. Kim SH, Lee SW, Lee GM, Lee BT, Yun ST, Kim SO. Monitoring of TiO_2-catalytic UV-LED photo-oxidation of cyanide contained in mine wastewater and leachate. *Chemosphere*. 2016;143:106-114.